

Towards the Explanation of Graph Neural Networks in Digital Pathology with Information Flows

Junchi Yu
Institute of Automation, CAS
Beijing, China

Tingyang Xu
Tencent AI Lab
Shenzhen, China

Ran He
Institute of Automation, CAS
Beijing, China

December 21, 2021

Abstract

As Graph Neural Networks (GNNs) are widely adopted in digital pathology, there is increasing attention to developing explanation models (explainers) of GNNs for improved transparency in clinical decisions. Existing explainers discover an explanatory subgraph relevant to the prediction. However, such a subgraph is insufficient to reveal all the critical biological substructures for the prediction because the prediction will remain unchanged after removing that subgraph. Hence, an explanatory subgraph should be not only necessary for prediction, but also sufficient to uncover the most predictive regions for the explanation. Such explanation requires a measurement of information transferred from different input subgraphs to the predictive output, which we define as information flow. In this work, we address these key challenges and propose IFEXPLAINER, which generates a necessary and sufficient explanation for GNNs. To evaluate the information flow within GNN’s prediction, we first propose a novel notion of predictiveness, named f -information, which is directional and incorporates the realistic capacity of the GNN model. Based on it, IFEXPLAINER generates the explanatory subgraph with maximal information flow to the prediction. Meanwhile, it minimizes the information flow from the input to the predictive result after removing the explanation. Thus, the produced explanation is necessarily important to

the prediction and sufficient to reveal the most crucial substructures. We evaluate IFEXPLAINER to interpret GNN’s predictions on breast cancer subtyping. Experimental results on the BRACS dataset show the superior performance of the proposed method.

1 Introduction

Recent advances in deep learning have greatly boosted the development of histopathological image analysis [7, 9]. Especially, it becomes increasingly popular to leverage the Graph Neural Networks (GNNs) to exploit the complex relationship between the biological entities in digital pathology images [16]. Various GNN-based methods are employed to facilitate clinical decisions such as cancer classification [18, 1, 41], histopathological image segmentation [40, 24, 10] and cancer detection [4]. Despite their success, the complex predictions made by GNNs are difficult for pathologists to understand [14, 32]. The clinical decisions based on GNNs cannot be fully trusted by the practitioners without interpretations of the predictions of GNNs. Although many efforts have been made to increase the transparency of Convolutional Neural Networks (CNNs) [8, 17, 11, 20], explaining the predictions of GNNs in digital pathology is still a nascent research topic.

Inspired by the developments in the explainability of GNNs, several explanation models (explainers) are implemented to recognize the important subgraph

of a biological entity-graph that is predictive to the GNN’s prediction [15]. However, the discovered subgraph is *insufficient* to fully uncover the explainability of GNNs since the GNNs probably make the same prediction after removing the subgraph. This indicates that these explainers potentially ignore some informative substructures to the prediction. Hence, apart from discovering an important subgraph for the explanation, explainers are also supposed to investigate whether removing the explanatory subgraph sufficiently leads to a different prediction. The recently proposed counterfactual-based explainers [22] partially address this issue by recognizing the minimal explanatory subgraph, if removed, that leads to an alternative prediction. However, the found subgraph may contain *unnecessarily* significant portion to the prediction. Suffering from the above two issues for recent GNN explainers, it motivates us to generate an ideal explainable subgraph which is not only *necessary* for GNNs to make a specific prediction, but also *sufficient* to uncover most crucial regions for the explanation.

Generating such an explanation requires identifying the contributions of different input substructures to the GNN’s prediction. To articulate this concept, we define the information transferred from the input to the prediction through the GNN models as the information flow. The information flow within GNNs is directional since we can only infer the underlying label of the input instead of vice versa. Moreover, it relies on a realistic capacity of GNN models to describe the information transfer. For example, a more powerful GNN predicts more easily than a less powerful one, which indicates the information flow varies in different GNN models. Existing methods [36, 35] tend to measure such information flow with mutual information. However, the mutual information is symmetric and only measures relevance between the input and its prediction without considering the modeling power of the GNN.

To measure the information flow within GNN’s prediction, we introduce a new notion of informativeness, namely f -Information, to evaluate the information flow within GNN’s prediction. Unlike mutual information, f -Information is directional and incorporates the realistic capacity of the GNN models.

Hence, we can identify the significance of different input substructures to the prediction by evaluating the corresponding information flows with f -Information. Based on f -Information, we emphasize the sufficient and necessary nature of the explanation and propose a novel explanation model, namely IFEXPLAINER, to faithfully explain the GNNs in digital pathology tasks. Specifically, it maximizes the information flow from the explanatory subgraph to the prediction while minimizing the information flow from the input to the prediction after removing the explanatory subgraph. The produced explanatory subgraph is thus necessarily important for the GNN to make the prediction and sufficiently change the prediction if removed. Therefore, the generated explanation faithfully interprets the GNN’s prediction by uncovering the most crucial substructures. Moreover, we introduce a tractable optimization scheme for IFEXPLAINER to explain the predictions of biological instances efficiently. Furthermore, to comprehensively evaluate the explainers in terms of necessity and sufficiency, we propose a set of pathologist-intelligible metrics based on subgraph-level separability. We employ IFEXPLAINER to explain the predictions of the GNN on breast cancer subtyping. Qualitative and quantitative results on BRACS dataset [25] show the superior performance of the proposed method.

The contributions of this work are summarized as follows:

- We propose a novel notion of f -Information to measure the information flows in the GNN’s prediction.
- We emphasize the necessary and sufficient nature of the explanation and propose the IFEXPLAINER to faithfully interpret GNN’s predictions by evaluating the information flows.
- We introduce a set of evaluation metrics based on subgraph level separability for the pathologist-intelligible evaluations.
- Extensive studies on the BRACS dataset verify the superior performance of the proposed method.

2 Related work

2.1 GNNs in Digital Pathology

Recent studies employ graph techniques to embed the biological entities such as cells, tissue regions, and patches into graph-structured data [2, 13]. Hence, GNN-based methods become popular to analyze such graph-structured data to facilitate medical decisions. A large body of these works focuses on the application of GNNs on cancer subtype classification, such as breast cancer classification [27, 3, 15], colorectal cancer classification [41, 31] and lung cancer classification [18, 1]. For example, the attention-based robust spatial filtering method is adopted to highlight the important cells to enhance the GNN’s performance on breast cancer subtype classification [32]. To exploit the hierarchical graph structure, Hact-net builds the tissue graph and cell graph to capture the cellular attributes at different levels [25]. Slide-Graph enriches the topological context of nodes via aggregating the local features in the cell graph [21]. Apart from the applications in cancer subtype classification, other works leverage GNN for histopathological image segmentation [4] and cancer detection [24]. GNN is also cooperated with the contrastive predictive coding for cancer detection in a weakly supervised manner using only labels at the tissue micro-arrays level [33]. While GNN has made tremendous progress in digital pathology, the explainability of GNN’s prediction is less explored. Several explanation methods of GNN are implemented to digital-pathology tasks [14]. However, the generated explanations do not uncover all the important substructures since they are insufficient to change the predictions if removed.

2.2 Explainability of GNNs

While the advancements in GNNs have revolutionized deep graph learning, the explainability of GNNs is lagged [35]. The discrete and combinatorial nature of graph-structured data hinders the development of GNNs’ explanation models [39, 36]. To this end, several methods have been proposed to discover an important subgraph of the input for the explanation [35, 23, 37, 12]. The gradient-based methods

such as GraphGRAD-CAM [26] and GraphGRAD-CAM++ [14] employ gradient values to evaluate the importance of each node based on CAM [30]. Similarly, GraphLRP decomposes the prediction into several terms concerning the nodes and edges [29]. Recently, it becomes popular to leverage the graph-pruning explainers to discover an explanatory subgraph that is most relevant to the static prediction. GNNEXPLAINER generates post-hoc explanations by maximizing the mutual information between the subgraphs and GNN’s predictions [35]. Furthermore, PGEXPLAINER learns a parametric model to generate explanations [23]. Similar to PGEXPLAINER, GraphMask generates the explanatory subgraph in a layer-wise manner [28]. Although these methods can generate explanations in the inductive setting, they heavily rely on the node embeddings from the GNNs [19], thus lacking the understanding of the biological graphs in digital pathology. The explainers such as SubgraphX [39] and XGNN [38] formulate the generation of explanations as a reinforcement learning task. However, it is time-consuming to verify the contribution of each node for large-scale biological graphs via reinforcement learning. While the graph-pruning explainers explain the individual predictions, the counterfactual-based explainers [22, 6] recognize a minimal subgraph, if moved, can lead to the drastic change in GNN’s prediction. While the discovered subgraph sufficiently changes the prediction if removed, it is may contain unnecessary important portions to the prediction.

3 Methodology

In this section, we begin with the formulation of the information flow as f -information. Then we introduce how information flows are used to comprehensively explain GNNs as IFEXPLAINER and how to optimize IFEXPLAINER. Finally, we discuss a novel evaluation metrics to measure how necessary and sufficient the selected subgraphs make the explanations of GNNs.

3.1 f -Information

Given two random variables X and Y , the mutual information $I(X, Y)$ is defined as follows:

$$I(X, Y) = \iint_{x,y} p(x, y) \log \frac{p(x, y)}{p(x)p(y)} dx dy \quad (1)$$

The mutual information is widely adopted to measure the relevance between random variables in representation learning. However, it is less appropriate to reason the explainability of GNNs with the mutual information. To explain GNN’s predictions, it is vital to investigate the information flow with GNNs, which is defined as the information transferred from the input to the output of GNNs. However, the mutual information is insufficient to represent such directional information flows. Specifically, the mutual information $I(X, Y)$ is symmetric, which means X and Y exchange equal information. This does not hold in GNN’s prediction since we can only infer the prediction Y from the input X instead of vice versa [34], which indicates that the information flow is directional. Moreover, the formulation of mutual information does not consider the modeling power of GNNs. In general, a more powerful GNN can infer Y from X more easily than a less powerful one, which shows the information flow from X to Y varies in different GNN models. The above analysis motivates us to find a proper metric to quantify the directional information flows in GNN’s prediction. Inspired by recent advances in machine learning [34], we propose a novel f -Information to exploit the information flow.

Definition 3.1 *Given X and Y be the input graph and the corresponding prediction, and f is the GNN that maps X to Y . The f -Information $I_f(X \rightarrow Y)$ is defined as follows:*

$$\begin{aligned} H_f(Y) &= E_y - \log f(y) \\ H_f(Y|X) &= E_{x,y} - \log f[x](y) \\ I_f(X \rightarrow Y) &= H_f(Y) - H_f(Y|X), \end{aligned} \quad (2)$$

where $f[x](y)$ is the output distribution of y after f receives the input x and $f(y) = E_x f[x](y)$ is the marginalized distribution of y . $H_f(Y)$ and $H_f(Y|X)$ are the f -entropy and conditional f -entropy. $I_f(X \rightarrow$

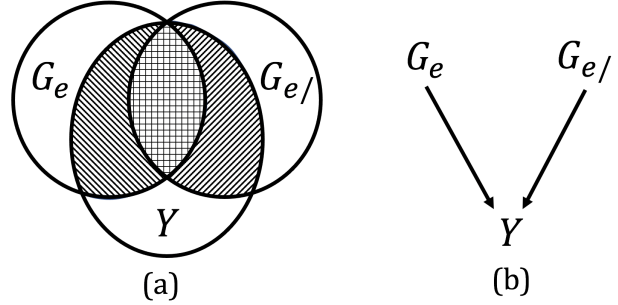


Figure 1: (a). The Venn diagram illustrating the relationship between the explanatory subgraph G_e , the complementary subgraph $G_{e\}$ and the prediction Y . The circles of G_e and $G_{e\}$ denote the entropy while the circle of Y is the f -entropy. The intersections of two circles represent $I_f(G_e \rightarrow Y)$ and $I_f(G_{e\} \rightarrow Y)$. When Y is known, the intersection of G_e and $G_{e\}$ vanishes due to the assumption that G_e and $G_{e\}$ are conditionally independent given Y . (b). The graphic model of IFEXPLAINER. The arrows represent directions of f -Information.

$Y)$ is the f -Information from X to Y and the arrow denotes the direction.

Similar to the predictive \mathcal{V} -Information [34], f -Information is a variational extension to the Shannon mutual information by incorporating the modeling power of the classifier. Differently, f -Information measures the information flow in a specific GNN while the \mathcal{V} -information focuses on learning optimal representations within a predictive family. Notice that f in Eq. 2 can be replaced by other neural networks such as CNN and RNN, and thus permits the application of f -Information to the explainability of other models. In our work, we focus on the explainability of GNNs in digital pathology.

3.2 Information Flow in GNN’s Explanation

A faithful explanation is supposed to be *necessary* for GNNs to make the prediction and *sufficient* to uncover most predictive regions. We formulate these conditions by measuring the corresponding information flows. Specifically, we recognize the explanatory

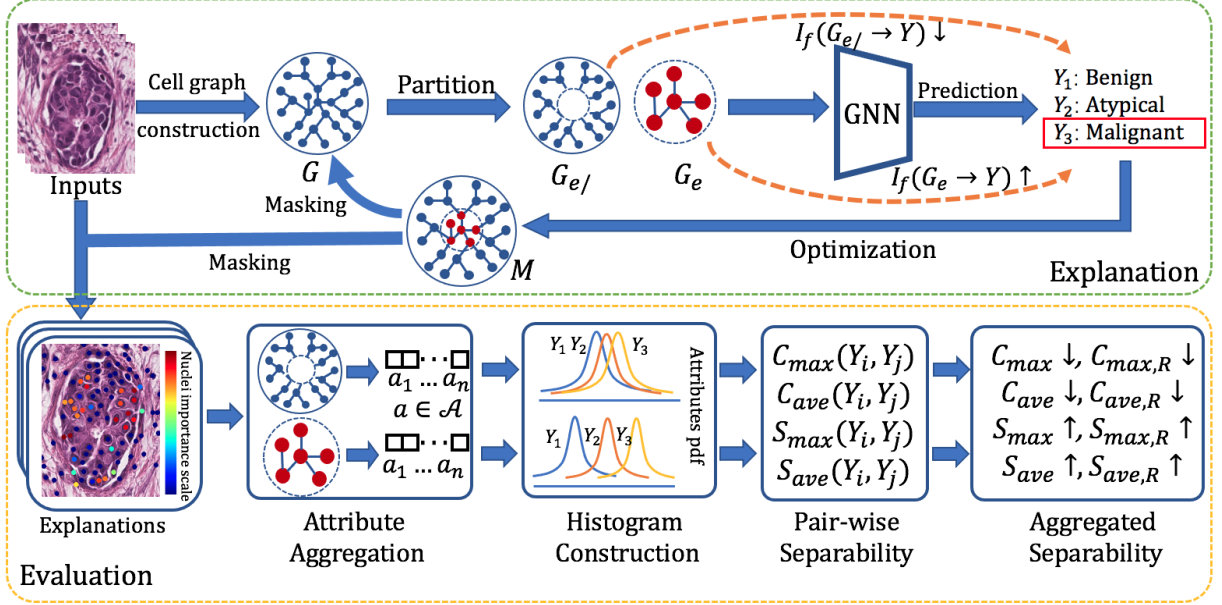


Figure 2: The framework of the proposed method. IFEXPLAINER generates necessary and sufficient explanations of GNNs by contradicting the information flows $I_f(G_e \rightarrow Y)$ and $I_f(G_{e\setminus} \rightarrow Y)$. To evaluate the necessity and sufficiency of the explanations, we aggregate the pathologist-intelligible attributes of G_e and $G_{e\setminus}$ respectively and calculate their inter-class separability.

subgraph of the input, which transfers maximal information flow to the GNN’s prediction. Meanwhile, we restrict the information flow from the input to the prediction after removing the explanatory subgraph.

Let $G \in \mathcal{G}$ and $Y \in \mathcal{Y}$ be the biological entity-graph such as the cell graph and the GNN’s prediction. f is the GNN to be explained, which maps G to Y . Define G_e and $G_{e\setminus}$ as the explanatory subgraph and the complementary subgraph after removing G_e from G . The relationship of G_e , $G_{e\setminus}$ and Y are shown in Figure 1 (a). In Figure 1 (a), the circle of Y represents the $H_f(Y)$. The circles of G_e and $G_{e\setminus}$ are $H(G_e)$ and $H(G_{e\setminus})$. And intersections of two circles denote the information flows which are measured by $I_f(G_e \rightarrow Y)$ and $I_f(G_{e\setminus} \rightarrow Y)$ respectively. As shown in Figure 1, Y receives information from both G_e and $G_{e\setminus}$ since the GNN f takes the whole structure of G to make the prediction. To produce a faithful explanation of the GNN, we need to maximize the information flow from G_e to Y , which is equal to maximize $I_f(G_e \rightarrow Y)$. Moreover, after

removing G_e from G , Y only receives the information flow from $G_{e\setminus}$. $G_{e\setminus}$ is less predictive to Y , as we hope G_e that reveals all the information for predicting Y . Intuitively, we hope the GNN will make a different prediction after removing G_e from G , which requires to minimize $I_f(G_{e\setminus} \rightarrow Y)$. The above analysis leads to a novel explainer, namely IFEXPLAINER, which leverages the **Information Flows** from different input substructures to the GNN’s predictions. We present the graphical model of IFEXPLAINER in Figure 1 (b) and the arrows indicate the directions of the information flows. The framework of IFEXPLAINER is shown in Figure 2. The objective of IFEXPLAINER is as follows:

$$\begin{aligned} & \max_{p_\theta(G_e)} I_f(G_e \rightarrow Y) - I_f(G_{e\setminus} \rightarrow Y) \\ & s.t. |G_e| \leq K, \end{aligned} \quad (3)$$

where $p_\theta(G_e) = \int_G p_\theta(G_e|G)p(G)dG$ is the parametric distribution of G_e and $|\cdot|$ denotes the number of nodes in G_e . We introduce a constant K to constrain

the size of G_e , and thus prevent from the trivial solution that $G_e = G$ and $G_{e\setminus} = \phi$. By introducing a Lagrange Multiplier β , we convert the constrained optimization problem into an unconstrained one:

$$\min_{G_e \sim p_\theta(G_e)} -I_f(G_e \rightarrow Y) + I_f(G_{e\setminus} \rightarrow Y) + \beta|G_e|. \quad (4)$$

3.3 Optimization Scheme for IFEXPLAINER

We introduce the optimization Scheme for minimizing the objective of IFEXPLAINER in Eq. 4. We first examine the f -Information terms in the objective:

$$\begin{aligned} \mathcal{L}_f &= -I_f(G_e \rightarrow Y) + I_f(G_{e\setminus} \rightarrow Y) \\ &= H_f(Y|G_e) - H_f(Y|G_{e\setminus}) \end{aligned} \quad (5)$$

Single Instance Explanation: The conditional f -entropy can be estimated by the batched data $\{(G_i, Y_i) | i = 1, \dots, N\}$ with provable guarantees. Please refer to Supplementary Materials for more details. Let $G_{e,i} \sim p_\theta(G_e|G_i)$ be the explanatory subgraph of G_i and $G_{e\setminus,i}$ is the corresponding complementary subgraph. We simplify the loss term in Eq. 5 as follows:

$$\mathcal{L}_f = \frac{1}{N} \sum_{i=1}^N \log f[G_{e\setminus,i}](Y_i) - \log f[G_{e,i}](Y_i). \quad (6)$$

Notice that $G_i \perp G_j$ for $i \neq j$, we plug Eq. 6 into Eq. 4 and further simplify the objective for the single-instance explanation:

$$\begin{aligned} \mathcal{L} &= \log f[G_{e\setminus,i}](Y_i) - \log f[G_{e,i}](Y_i) + \beta|G_{e,i}| \\ &= \mathcal{L}_f + \beta|G_{e,i}|. \end{aligned} \quad (7)$$

As $f[G_{e\setminus,i}](Y_i) \in [0, 1]$, minimizing $\log f[G_{e\setminus,i}](Y_i)$ probably results in the negative infinity, leading to an unstable training process. Thus, we replace this term with a minimax loss:

$$\begin{aligned} \mathcal{L}_f &= \max[\log f[G_{e\setminus,i}](Y_i), \min_{j \neq i}(\log f[G_{e\setminus,i}](Y_j))] \\ &\quad - \log f[G_{e,i}](Y_i), \end{aligned} \quad (8)$$

Continuous Relaxation. However, it is still intractable to minimize the objective in Eq. 7, mostly due to the discrete and irregular nature of the graph-structured data. Moreover, sampling the explanatory subgraph is computationally inefficient since a graph has exponentially many subgraphs. Thus, we consider learning a differentiable soft mask to generate the explanatory subgraph. Different from the practice in GNNEXPLAINER [35], we do not mask node features since we only highlight the critical topology of the biological graph to GNN’s prediction, which is more intuitive and human-intelligible [39]. Given an input graph G with n nodes, we obtain G_e by applying a node mask $M \in \mathcal{R}^n$ to G . The elements of M are bounded in $[0, 1]$, which indicates the corresponding nodes’ importance scores. And we mask G with $1 - M$ to obtain $G_{e\setminus}$. Note that M is a soft mask with continuous values instead of a binary mask, we further employ an entropy constraint to encourage discrete values in M [23]:

$$\mathcal{L}_{ent} = \sum_{i=1}^n -M_i \log M_i - (1 - M_i) \log(1 - M_i), \quad (9)$$

where M_i is the i -th element of M . We further convert the size constraint $|G_e|$ in Eq. 7 to the constraint on the summation of the elements in M : $\mathcal{L}_{size} = |G_e| = \sum_{i=1}^n M_i$. Thus, the total loss function of IFEXPLAINER is:

$$\mathcal{L} = \mathcal{L}_f + \beta \mathcal{L}_{size} + \gamma \mathcal{L}_{ent}, \quad (10)$$

where β and γ are hyper-parameters.

3.4 Subgraph-level Evaluation Metrics

We propose a set of pathologist-intelligible evaluation metrics for the explanations of GNNs on breast cancer subtyping with the relevant pathological attributes. Our evaluation metrics aggregate the pathological attributes of the nuclei for the explanatory and complementary subgraphs, and evaluate their inter-class separability scores at the subgraph level. Hence, they provide comprehensive assessments considering the necessary and sufficient nature

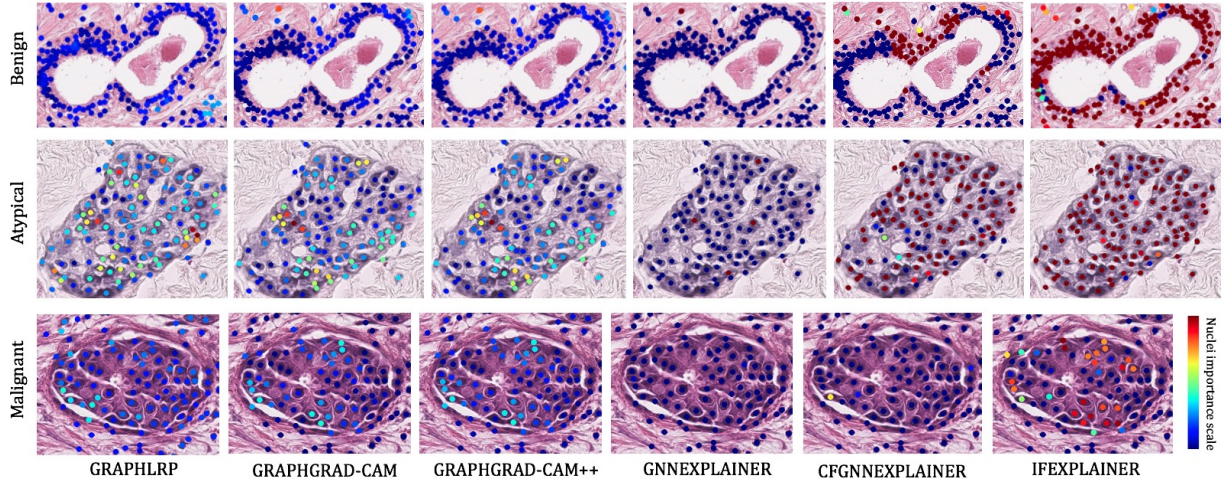


Figure 3: Explanations for the breast cancer subtyping. The rows and columns represent cancer subtypes and the explanation results of different explainers. The important nuclei are highlighted according to their importance scores.

of the explanations. And they are less affected by the diverse numbers of nuclei in different cell graphs.

Subgraph-level Attribute Aggregation: Suppose we explain the prediction of a cell graph, where the nodes and edges denote nuclei and cellular interactions. Given the explanatory subgraph G_e and the complementary subgraph G_{e^c} , we aggregate their nuclei attributes $a \in \mathcal{A}$ of G_e and G_{e^c} via weighted summation:

$$a_{G_e}^k = \sum_{i \in \mathcal{E}} M_i a_i / \sum_{i \in \mathcal{E}} M_i, a_{G_{e^c}}^k = \sum_{i \in \mathcal{E}^c} M_i a_i / \sum_{i \in \mathcal{E}^c} M_i \quad (11)$$

where \mathcal{E} is the set of the top $k\%$ important nuclei in the input graph G and k is the sparsity of G_e . M_i denotes the importance of the i -th nucleus in \mathcal{E} . $a_{G_e}^k$ and $a_{G_{e^c}}^k$ are the aggregated attributed for G_e and G_{e^c} .

Histogram Construction: For the cancer subtype $t \in \mathcal{T}$ and $k \in \mathcal{K}$, we construct the histograms of $a_{G_e}^k$ and $a_{G_{e^c}}^k$, denoted as $H_t^k(a_{G_e})$ and $H_t^k(a_{G_{e^c}})$. Then, we transform the histograms into the probability density functions.

Separability Scores: The explanatory subgraphs encourage the inter-class separability of $H_t^k(a_{G_e})$ while reduce inter-class separability of $H_t^k(a_{G_{e^c}})$. Hence, we calculate the Wassertein distance between

the probability density functions to evaluate the pair-wise class separability.

We first compute the predictive separability scores S of G_e . Given a class pair (t_x, t_y) , we compute the Wassertein distance between $H_{t_x}^k(a_{G_e})$ and $H_{t_y}^k(a_{G_e})$. Then, we average the distances of attributes $a \in \mathcal{A}_c$ which belong to the same pathological concepts $c \in \mathcal{C}$, and obtain the concept distance $d_c^k(t_x, t_y)$ under the sparsity k . Moreover, we compute the AUC of $d_c^k(t_x, t_y)$ across different k , which is denoted as $D_c(t_x, t_y)$. The maximal and average pair-wise metrics of S are calculated as follows:

$$S_{max}(t_x, t_y) = \max_{c \in \mathcal{C}} D_c(t_x, t_y) \quad (12)$$

$$S_{ave}(t_x, t_y) = \frac{1}{|\mathcal{C}|} \sum_{c \in \mathcal{C}} D_c(t_x, t_y)$$

To evaluate the separability across all the class pairs, we sum up the pair-wise metrics for the aggregated metrics: S_{max} and S_{ave} . We further consider the $R(t_x, t_y)$ of misclassifying a sample of class t_x into t_y and vice versa, leading to the risk-aggregated metrics: $S_{max,R}$, $S_{ave,R}$. We empirically set the risks following [14]. Thus, the predictive separability scores S of G_e consist of 1. the maximal and average pair-wise metrics: $S_{max}(t_x, t_y)$ and $S_{ave}(t_x, t_y)$; 2. the aggregated metrics: S_{max} and S_{ave} ; 3. the risk-aggregated

Table 1: Quantitative results of different explainers. We compare the average and maximal metrics of the pair-wise and aggregated separability scores.

Class pair	B vs. A				B vs. M		A vs. M		B vs. A vs. M			
	Metric	$C_{max} \downarrow$	$S_{max} \uparrow$	$C_{max} \downarrow$	$S_{max} \uparrow$	$C_{max} \downarrow$	$S_{max} \uparrow$	$C_{max} \downarrow$	$S_{max} \uparrow$	$C_{max,R} \downarrow$	$S_{max,R} \uparrow$	
GRAPHGRAD-CAM	0.393	0.328	0.310	0.453	0.477	<u>0.598</u>	1.180	1.379	1.489	1.832		
GRAPHGRAD-CAM++	0.404	0.318	<u>0.307</u>	0.457	0.477	0.619	1.188	<u>1.394</u>	1.495	<u>1.850</u>		
GRAPHLRP	0.360	0.268	0.310	0.313	0.610	0.310	1.28	0.892	1.590	1.205		
GNNEXPLAINER	0.373	0.307	0.285	0.479	0.536	0.401	1.194	1.187	1.480	1.666		
CFGNNEXPLAINER	0.350	0.226	0.304	0.514	0.475	0.41	1.129	1.15	1.433	1.664		
IFExplainer	<u>0.338</u>	0.355	0.290	0.521	0.465	0.542	1.093	1.418	1.383	1.939		
IFExplainer w/o \mathcal{L}_{size}	0.378	<u>0.345</u>	0.319	0.492	0.519	0.407	1.216	1.244	1.534	1.736		
IFExplainer w/o \mathcal{L}_{ent}	0.336	0.317	0.322	<u>0.510</u>	<u>0.474</u>	0.467	<u>1.121</u>	1.294	<u>1.443</u>	1.803		
Class pair	B vs. A				B vs. M		A vs. M		B vs. A vs. M			
	Metric	$C_{ave} \downarrow$	$S_{ave} \uparrow$	$C_{ave} \downarrow$	$S_{ave} \uparrow$	$C_{ave} \downarrow$	$S_{ave} \uparrow$	$C_{ave} \downarrow$	$S_{ave} \uparrow$	$C_{ave,R} \downarrow$	$S_{ave,R} \uparrow$	
GRAPHGRAD-CAM	0.272	0.247	0.212	0.302	0.319	<u>0.335</u>	0.803	0.884	1.015	1.187		
GRAPHGRAD-CAM++	0.276	0.249	<u>0.208</u>	0.306	0.319	0.343	0.803	0.897	1.011	1.203		
GRAPHLRP	0.253	0.227	0.257	0.197	0.356	0.235	0.866	0.659	1.123	0.857		
GNNEXPLAINER	0.241	0.240	0.249	<u>0.343</u>	0.323	0.32	0.813	0.903	1.062	1.247		
CFGNNEXPLAINER	0.258	0.188	0.213	0.338	0.297	0.277	0.768	0.803	0.981	1.141		
IFExplainer	0.251	0.257	0.207	0.338	0.290	0.327	0.748	0.922	0.955	1.261		
IFExplainer w/o \mathcal{L}_{size}	<u>0.246</u>	<u>0.253</u>	0.270	0.273	0.343	0.327	0.858	0.854	1.127	1.127		
IFExplainer w/o \mathcal{L}_{ent}	0.263	0.246	0.216	0.341	<u>0.296</u>	0.325	<u>0.775</u>	<u>0.912</u>	<u>0.991</u>	<u>1.253</u>		

metrics: $S_{max,R}$, $S_{ave,R}$.

Following the steps of calculating the predictive separability scores, we further compute the counterfactual separability scores C of $G_e \setminus$. Similarly, the counterfactual separability scores C consist of 1. the maximal and average pair-wise metrics: $C_{max}(t_x, t_y)$ and $C_{ave}(t_x, t_y)$; 2. the aggregated metrics: C_{max} and C_{ave} ; 3. the risk-aggregated metrics: $C_{max,R}$, $C_{ave,R}$. Please refer to Supplementary Materials for more details.

4 Experiments

4.1 Evaluation Metrics

Fidelity: The fidelity scores evaluate how the explanations are faithful to the GNN model [39]. We define the Fidelity+ score as the agreement between the original prediction and predictions of the explanatory subgraphs. The Fidelity- score is the agreement between the original predictions and the predictions after removing the explanatory subgraphs. Let y_i be the prediction of the i -th graph. $\hat{y}_i^{G_e}$ and $\hat{y}_i^{G_e \setminus}$ are the predictions of the explanatory and complementary subgraph of the i -th graph. The fidelity scores are computed as: $Fidelity+ = \frac{1}{N} \sum_{i=1}^N \mathbb{1}(y_i =$

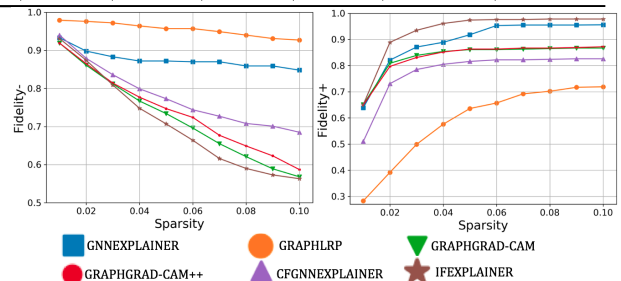


Figure 4: A comparison on the fidelity scores of different explainers. IFEXPLAINER achieves best Fidelity-(\downarrow) and Fidelity+(\uparrow) on most sparsity scores.

$\hat{y}_i^{G_e}$), $Fidelity- = \frac{1}{N} \sum_{i=1}^N \mathbb{1}(y_i = \hat{y}_i^{G_e \setminus})$. Here $\mathbb{1}(y_i = \hat{y}_i^{G_e})$ is the indicator function which outputs 1 if $y_i = \hat{y}_i^{G_e}$ and 0 otherwise. Following [14], we filter out the misclassified samples. For a fair comparison, the fidelity scores should be evaluated at the same level of sparsity, which is defined as the fraction of nodes in the explanatory subgraph: $k = |G_e|/|G|$. We set $k \in \{1\%, 2\%, \dots, 10\%\}$ in the experiment.

Separability: We further evaluate the separability scores of the explanations introduced in Section 3.4. Specifically, the higher predictive separability scores S indicate that the explanatory subgraphs G_e are easier to classify. Hence, G_e contains necessarily important information for the prediction. Mean-

while, the lower counterfactual separability scores C show that the explanatory subgraphs $G_{e\setminus}$ are difficult to classify, leading to a different prediction.

4.2 Dataset and Settings

We employ the BReAst Cancer Subtyping (BRACS) dataset [25] for the experiments. It consists of 4931 RoIs at $40\times$ magnification sampled from 325 H&E stained breast carcinoma whole-slides, and each RoI contains 1468 nuclei on average. We transform the RoIs into cell graphs following [13]. The labels of the cell graphs are Benign (B): normal, benign and usual ductal hyperplasia; Atypical (A): flat epithelial atypia and atypical ductal hyperplasia; and Malignant (M): ductal carcinoma *in situ* and invasive[14]. The training, validation and test sets contain 3162, 602 and 626 cell graphs.

We explain the pre-trained GNN which predicts the breast cancer subtypes of the cell graphs. It achieves 74.2% weighted F1-score on the test set. We set $\beta = 0.05$ and $\gamma = 0.1$ for training IFEXPLAINER. Please refer to Supplementary Materials for more details on the experiments of hyperparameters.

4.3 Baselines

GRAPHLRP [29]: GRAPHLRP outputs the importance score of each node in graph classification based on Layer-wise Relevance Propagation (LRP) [5]. We employ GRAPHLRP to identify the importance scores of important nuclei in breast cancer subtyping.

GRAPHGRAD-CAM: Based on GRAD-CAM [30], GRAPHGRAD-CAM computes the gradients w.r.t different GNN layers to output the node importance scores for the explanations of GNNs [26].

GRAPHGRAD-CAM++: GRAPHGRAD-CAM++ considers the spatial contribution in the computation of the weighted gradients for the improved node importance scores. We follow the implementation in [14] to obtain the nuclei importance score.

GNNEXPLAINER [35, 15]: GNNEXPLAINER maximizes the mutual information

between the distribution of the potential explanatory subgraphs and the original predictions for the explanations.

CFGNNEXPLAINER [22]: CFGNNEXPLAINER recognizes a minimal subgraph of the input, if removed, would lead to a drastic change in the prediction.

4.4 Performance

We employ IFEXPLAINER and the baseline methods to interpret the predictions of the GNN for breast cancer subtyping. As shown in Table 1, IFEXPLAINER achieves higher predictive separability scores S over the baselines on most pair-wise metrics and all the aggregated metrics. This shows that IFEXPLAINER generates explanatory subgraphs with higher inter-class separability, and thus are most important to the predictions. Moreover, IFEXPLAINER outperforms the baselines with lower counterfactual separability scores C on most pair-wise and aggregated metrics. Hence, the complementary subgraphs obtained by removing the explanatory subgraphs are least separable and most likely cause the prediction changes. Noticeably, the predictive separability scores are consistently higher than the corresponding counterfactual separability scores for IFEXPLAINER. This shows that IFEXPLAINER uncovers the most important nuclei for the cancer subtype. However, most baseline methods have a higher C_{ave} than S_{ave} for the class pair (B v.s. A). This shows that the explanatory subgraphs produced by IFEXPLAINER identify most necessarily and sufficiently important nuclei for the breast cancer subtyping.

We further compare the fidelity scores of different methods. As the sparsity increases, the Fidelity-score of IFEXPLAINER declines drastically in Figure 4. This shows that the removal of the explanation is most likely to cause the prediction change. IFEXPLAINER also outperforms the baselines on the Fidelity+ scores, which indicates the produced explanation is most important to the prediction. Noticeably, the Fidelity-score of GNNEXPLAINER declines slowly as the sparsity increases. Thus, GNNEXPLAINER ignores some predictive nuclei for the

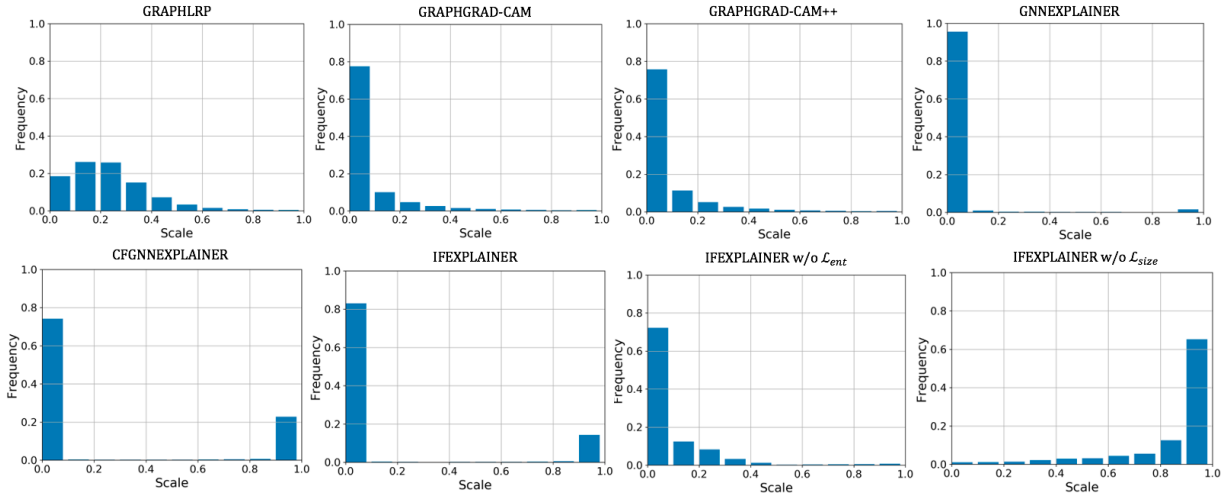


Figure 5: The distributions of nuclei importance scores generated by different explainers. prediction.

4.5 Visualization

We visualize the nuclei importance scores generated by different explanation methods. As shown in Figure 3, IFEXPLAINER generates almost binarized importance scores and emphasizes the nuclei leading to the predictions. Similarly, GNNEXPLAINER and CFGNNEXPLAINER also generate binarized node importance scores. However, the results of GNNEXPLAINER are less interpretable since almost all nuclei are categorized as unimportant to the breast cancer subtypes. And CFGNNEXPLAINER only attaches importance to a small portion of nuclei that are relevant to the predictions. Noticeably, GRAPHLRP and gradient-based methods such as GRAPHGRAD-CAM and GRAPHGRAD-CAM++ consistently highlight similar regions. Unlike IFEXPLAINER, their importance maps are less pathologist-intelligible since most nuclei are attached to low importance scores.

We further analyze the distributions of nuclei importance scores produced by different methods. Ideally, the importance scores are binary values, indicating whether the nucleus is informative for the prediction. In practice, the explanation models either evaluate the nuclei importance heuristically, or optimize a differentiable node mask. Hence, the out-

put importance scores are continuous values between $[0,1]$. However, the new semantic meaning or noises introduced by the continuous importance scores prevent the pathologists from reasoning the explainability of GNNs. Thus, it is important to generate binarized importance scores. As shown in Figure 5, GRAPHLRP and the gradient-based methods generate continuous importance scores and assign low importance to most nuclei. GNNEXPLAINER attaches low importance to most nuclei, which is less interpretable. Differently, both CFGNNEXPLAINER and IFEXPLAINER generate almost binarized importance scores. However, IFEXPLAINER outperforms CFGNNEXPLAINER in qualitative and quantitative studies since the explanation produced by CFGNNEXPLAINER is not necessarily important to the prediction.

4.6 Ablation Study

To evaluate the influences of \mathcal{L}_{size} and \mathcal{L}_{ent} on the produced explanations, we individually remove these terms in the objective, which leads to two variant models, namely IFEXPLAINER w/o \mathcal{L}_{size} and IFEXPLAINER w/o \mathcal{L}_{ent} . We first evaluate the generated explanations of these methods in terms of separability scores. As shown in Table 1, IFEXPLAINER outperforms the variants on most pair-wise and aggregated separability scores, which shows the efficacy

of \mathcal{L}_{size} and \mathcal{L}_{ent} . Moreover, we study the distributions of nuclei importance scores of these variants. As shown in Figure 4, IFEXPLAINER w/o \mathcal{L}_{size} attaches high importance to most nuclei as there is no constraint on the sizes of the explanatory subgraphs. And IFEXPLAINER w/o \mathcal{L}_{ent} can not generate binary importance scores without the entropy constraint.

5 Discussions

Potential Negative Impacts: Our explainer is designed for improved transparency in GNN-based clinical decisions. The concern is that this technique, if not adequately used under administration, may lead to the privacy leakage.

Limitations: IFEXPLAINER generates the customized explanation to the prediction of each biological instance without access to the node embeddings inside the black-box GNNs. Thus, it can be easily adapted to interpret various GNN models in digital pathology tasks. However, this also limits the usage of our model in inductive settings. We leave it in our future work.

6 Conclusion

In this work, we emphasize the necessary and sufficient nature of the explanations and propose a novel explainer of GNN in digital pathology, namely IFEXPLAINER. IFEXPLAINER exploits the information flows from different input substructures to the prediction with the notion of f -Information, and generates faithful explanation to the GNN’s prediction. We also propose a set of evaluation metrics based on subgraph-level separability for the comprehensive assessments to the explanation models. Experimental results on the BRACS dataset show the superior performance of the proposed method.

References

[1] Mohammed Adnan, Shivam Kalra, and Hamid R Tizhoosh. Representation learning of histopathology

images using graph neural networks. In *Proceedings of the IEEE/CVF Conference on Computer Vision and Pattern Recognition Workshops*, pages 988–989, 2020. 1, 3

[2] David Ahmedt-Aristizabal, Mohammad Ali Armin, Simon Denman, Clinton Fookes, and Lars Petersson. A survey on graph-based deep learning for computational histopathology. *arXiv preprint arXiv:2107.00272*, 2021. 3

[3] Deepak Anand, Shrey Gadiya, and Amit Sethi. Histograms: graphs in histopathology. In *Medical Imaging 2020: Digital Pathology*, volume 11320, page 113200O. International Society for Optics and Photonics, 2020. 3

[4] Valentin Anklin, Pushpak Pati, Guillaume Jaume, Behzad Bozorgtabar, Antonio Foncubierta-Rodríguez, Jean-Philippe Thiran, Mathilde Sibony, Maria Gabrani, and Orcun Goksel. Learning whole-slide segmentation from inexact and incomplete labels using tissue graphs. *arXiv preprint arXiv:2103.03129*, 2021. 1, 3

[5] Sebastian Bach, Alexander Binder, Grégoire Montavon, Frederick Klauschen, Klaus-Robert Müller, and Wojciech Samek. On pixel-wise explanations for non-linear classifier decisions by layer-wise relevance propagation. *PloS one*, 10(7):e0130140, 2015. 9

[6] Mohit Bajaj, Lingyang Chu, Zi Yu Xue, Jian Pei, Lanjun Wang, Peter Cho-Ho Lam, and Yong Zhang. Robust counterfactual explanations on graph neural networks. *arXiv preprint arXiv:2107.04086*, 2021. 3

[7] Pedro J Ballester and Javier Carmona. Artificial intelligence for the next generation of precision oncology, 2021. 1

[8] Alexander Binder, Michael Bockmayr, Miriam Hägele, Stephan Wienert, Daniel Heim, Katharina Hellweg, Albrecht Stenzinger, Laura Parlow, Jan Budczies, Benjamin Goeppert, et al. Towards computational fluorescence microscopy: machine learning-based integrated prediction of morphological and molecular tumor profiles. *arXiv preprint arXiv:1805.11178*, 2018. 1

[9] Lisa Browning, Richard Colling, Emad Rakha, Nasir Rajpoot, Jens Rittscher, Jacqueline A James, Manuel Salto-Tellez, David RJ Snead, and Clare Verrill. Digital pathology and artificial intelligence will be key to supporting clinical and academic cellular pathology through covid-19 and future crises: the

- pathlake consortium perspective. *Journal of clinical pathology*, 74(7):443–447, 2021. 1
- [10] Simon Graham, Quoc Dang Vu, Shan E Ahmed Raza, Ayesha Azam, Yee Wah Tsang, Jin Tae Kwak, and Nasir Rajpoot. Hover-net: Simultaneous segmentation and classification of nuclei in multi-tissue histology images. *Medical Image Analysis*, 58:101563, 2019. 1
- [11] Mara Graziani, Vincent Andrearczyk, Stéphane Marchand-Maillet, and Henning Müller. Concept attribution: Explaining cnn decisions to physicians. *Computers in biology and medicine*, 123:103865, 2020. 1
- [12] Qiang Huang, Makoto Yamada, Yuan Tian, Dinesh Singh, Dawei Yin, and Yi Chang. Graphlime: Local interpretable model explanations for graph neural networks. *arXiv preprint arXiv:2001.06216*, 2020. 3
- [13] Guillaume Jaume, Pushpak Pati, Valentin Anklin, Antonio Foncubierta, and Maria Gabrani. Histocartography: A toolkit for graph analytics in digital pathology. In *MICCAI Workshop on Computational Pathology*, pages 117–128. PMLR, 2021. 3, 9
- [14] Guillaume Jaume, Pushpak Pati, Behzad Borzogtabar, Antonio Foncubierta, Anna Maria Anniciello, Florinda Feroce, Tilman Rau, Jean-Philippe Thiran, Maria Gabrani, and Orcun Goksel. Quantifying explainers of graph neural networks in computational pathology. In *Proceedings of the IEEE/CVF Conference on Computer Vision and Pattern Recognition*, pages 8106–8116, 2021. 1, 3, 7, 8, 9
- [15] Guillaume Jaume, Pushpak Pati, Antonio Foncubierta-Rodríguez, Florinda Feroce, Giosue Scognamiglio, Anna Maria Anniciello, Jean-Philippe Thiran, Orcun Goksel, and Maria Gabrani. Towards explainable graph representations in digital pathology. *arXiv preprint arXiv:2007.00311*, 2020. 2, 3, 9
- [16] Thomas N Kipf and Max Welling. Semi-supervised classification with graph convolutional networks. *arXiv preprint arXiv:1609.02907*, 2016. 1
- [17] Bruno Korbar, Andrea M Olofson, Allen P Miralflor, Catherine M Nicka, Matthew A Suriawinata, Lorenzo Torresani, Arief A Suriawinata, and Saeed Hassanpour. Looking under the hood: Deep neural network visualization to interpret whole-slide image analysis outcomes for colorectal polyps. In *Proceedings of the IEEE Conference on Computer Vision and Pattern Recognition Workshops*, pages 69–75, 2017. 1
- [18] Ruoyu Li, Jiawen Yao, Xinliang Zhu, Yeqing Li, and Junzhou Huang. Graph cnn for survival analysis on whole slide pathological images. In *International Conference on Medical Image Computing and Computer-Assisted Intervention*, pages 174–182. Springer, 2018. 1, 3
- [19] Wanyu Lin, Hao Lan, and Baochun Li. Generative causal explanations for graph neural networks. *arXiv preprint arXiv:2104.06643*, 2021. 3
- [20] Ming Y Lu, Drew FK Williamson, Tiffany Y Chen, Richard J Chen, Matteo Barbieri, and Faisal Mahmood. Data-efficient and weakly supervised computational pathology on whole-slide images. *Nature Biomedical Engineering*, 5(6):555–570, 2021. 1
- [21] Wenqi Lu, Simon Graham, Mohsin Bilal, Nasir Rajpoot, and Fayyaz Minhas. Capturing cellular topology in multi-gigapixel pathology images. In *Proceedings of the IEEE/CVF Conference on Computer Vision and Pattern Recognition Workshops*, pages 260–261, 2020. 3
- [22] Ana Lucic, Maartje ter Hoeve, Gabriele Tolomei, Maarten de Rijke, and Fabrizio Silvestri. Cf-gnnexplainer: Counterfactual explanations for graph neural networks. *arXiv preprint arXiv:2102.03322*, 2021. 2, 3, 9
- [23] Dongsheng Luo, Wei Cheng, Dongkuan Xu, Wenchao Yu, Bo Zong, Haifeng Chen, and Xiang Zhang. Parameterized explainer for graph neural network. *arXiv preprint arXiv:2011.04573*, 2020. 3, 6
- [24] Yigit Ozen, Selim Aksoy, Kemal Kösemehmetoğlu, Sevgen Önder, and Ayşegül Üner. Self-supervised learning with graph neural networks for region of interest retrieval in histopathology. In *2020 25th International Conference on Pattern Recognition (ICPR)*, pages 6329–6334. IEEE, 2021. 1, 3
- [25] Pushpak Pati, Guillaume Jaume, Lauren Alisha Fernandes, Antonio Foncubierta-Rodríguez, Florinda Feroce, Anna Maria Anniciello, Giosue Scognamiglio, Nadia Brancati, Daniel Riccio, Maurizio Di Bonito, et al. Hact-net: A hierarchical cell-to-tissue graph neural network for histopathological image classification. In *Uncertainty for Safe Utilization of Machine Learning in Medical Imaging, and Graphs in Biomedical Image Analysis*, pages 208–219. Springer, 2020. 2, 3, 9

- [26] Phillip E Pope, Soheil Kolouri, Mohammad Rostami, Charles E Martin, and Heiko Hoffmann. Explainability methods for graph convolutional neural networks. In *Proceedings of the IEEE/CVF Conference on Computer Vision and Pattern Recognition*, pages 10772–10781, 2019. **3, 9**
- [27] Sungmin Rhee, Seokjun Seo, and Sun Kim. Hybrid approach of relation network and localized graph convolutional filtering for breast cancer subtype classification. *arXiv preprint arXiv:1711.05859*, 2017. **3**
- [28] Michael Sejr Schlichtkrull, Nicola De Cao, and Ivan Titov. Interpreting graph neural networks for nlp with differentiable edge masking. *arXiv preprint arXiv:2010.00577*, 2020. **3**
- [29] Robert Schwarzenberg, Marc Hübner, David Harbecke, Christoph Alt, and Leonhard Hennig. Layerwise relevance visualization in convolutional text graph classifiers. *arXiv preprint arXiv:1909.10911*, 2019. **3, 9**
- [30] Ramprasaath R Selvaraju, Michael Cogswell, Abhishek Das, Ramakrishna Vedantam, Devi Parikh, and Dhruv Batra. Grad-cam: Visual explanations from deep networks via gradient-based localization. In *Proceedings of the IEEE international conference on computer vision*, pages 618–626, 2017. **3, 9**
- [31] Linda Studer, Jannis Wallau, Heather Dawson, Inti Zlobec, and Andreas Fischer. Classification of intestinal gland cell-graphs using graph neural networks. In *2020 25th International Conference on Pattern Recognition (ICPR)*, pages 3636–3643. IEEE, 2021. **3**
- [32] Mookund Sureka, Abhijeet Patil, Deepak Anand, and Amit Sethi. Visualization for histopathology images using graph convolutional neural networks. In *2020 IEEE 20th International Conference on Bioinformatics and Bioengineering (BIBE)*, pages 331–335. IEEE, 2020. **1, 3**
- [33] Jingwen Wang, Richard J Chen, Ming Y Lu, Alexander Baras, and Faisal Mahmood. Weakly supervised prostate tma classification via graph convolutional networks. In *2020 IEEE 17th International Symposium on Biomedical Imaging (ISBI)*, pages 239–243. IEEE, 2020. **3**
- [34] Yilun Xu, Shengjia Zhao, Jiaming Song, Russell Stewart, and Stefano Ermon. A theory of usable information under computational constraints. *arXiv preprint arXiv:2002.10689*, 2020. **4**
- [35] Rex Ying, Dylan Bourgeois, Jiaxuan You, Marinka Zitnik, and Jure Leskovec. Gnnexplainer: Generating explanations for graph neural networks. *Advances in neural information processing systems*, 32:9240, 2019. **2, 3, 6, 9**
- [36] Junchi Yu, Tingyang Xu, Yu Rong, Yatao Bian, Junzhou Huang, and Ran He. Graph information bottleneck for subgraph recognition. *International Conference on Learning Representations*, 2021. **2, 3**
- [37] Junchi Yu, Tingyang Xu, Yu Rong, Yatao Bian, Junzhou Huang, and Ran He. Recognizing predictive substructures with subgraph information bottleneck. *IEEE Transactions on Pattern Analysis and Machine Intelligence*, 2021. **3**
- [38] Hao Yuan, Jiliang Tang, Xia Hu, and Shuiwang Ji. Xgnn: Towards model-level explanations of graph neural networks. In *Proceedings of the 26th ACM SIGKDD International Conference on Knowledge Discovery & Data Mining*, pages 430–438, 2020. **3**
- [39] Hao Yuan, Haiyang Yu, Jie Wang, Kang Li, and Shuiwang Ji. On explainability of graph neural networks via subgraph explorations. *arXiv preprint arXiv:2102.05152*, 2021. **3, 6, 8**
- [40] Yushan Zheng, Bonan Jiang, Jun Shi, Haopeng Zhang, and Fengying Xie. Encoding histopathological wsis using gnn for scalable diagnostically relevant regions retrieval. In *International Conference on Medical Image Computing and Computer-Assisted Intervention*, pages 550–558. Springer, 2019. **1**
- [41] Yanning Zhou, Simon Graham, Navid Alemi Koohbanani, Muhammad Shaban, Pheng-Ann Heng, and Nasir Rajpoot. Cgc-net: Cell graph convolutional network for grading of colorectal cancer histology images. In *Proceedings of the IEEE/CVF International Conference on Computer Vision Workshops*, pages 0–0, 2019. **1, 3**